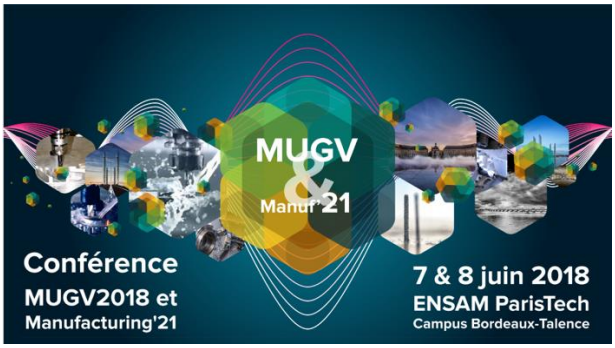

Hybrid Position/Force Control with Compliant Wrist for Grinding

Kamal MOHY EL DINE, Laurent LEQUIEVRE, Juan-Antonio CORRALES-RAMON, Youcef MEZOUAR, Jean-Christophe FAUROUX

Institut Pascal, SIGMA Clermont, Université Clermont Auvergne, CNRS, F-63000 Clermont-Ferrand, France. Mail : kamal.mohy_el_dine@sigma-clermont.fr, laurent.lequievre@univ-bpclermont.fr, juan-antonio.corrales-ramon@sigma-clermont.fr, youcef.mezouar@sigma-clermont.fr, jean-christophe.fauroux@sigma-clermont.fr

Abstract: Within the framework of the H2020 European Project 'Bots2ReC' (roBots to Re-Construction) ("Robots to Re-Construction", 2017), an automated system for the removal of asbestos from a real world rehabilitation site will be developed. The system will consist of multiple robotic units, each one is composed of a mobile platform and a robotic arm with a rotative abrasive tool. In this paper, only the arm control is considered, and the smooth position-force controller presented in (Mohy El Dine, 2017) is validated on a Kuka LWR lightweight robotic arm. The arm is equipped with force/torque sensor, camera and spindle with a grinding tool. The mentioned controller reconsiders the position, force and impedance control strategies together from a practical point of view to achieve the real grinding task. The experimental validation shows the efficiency, advantages and drawbacks of the proposed controller and it draws conclusions about the main factors that affect the wall grinding operation and its quality.

Keywords: Hybrid force-position control, impedance control, grinding.

1 Introduction

Over the past few decades various automation concepts for construction have been developed as a response to the strongly growing civil engineering industry. The number of robots implemented in construction and demolition industries is in continuous growth as the International Federation of Robotics (IFR) states that the number of robots and automatic systems supplied in 2015 was 568 unit and expected to reach 2,800 units in 2019 (IFR, 2016). However, construction tasks remain a challenge for robots, as they require varied techniques, specific tools, highly skilled operators and they take place in varied and complex environments that require advanced perception capacities. At this time, the majority of the tasks is still performed manually using conventional electrical and hydraulic tools. However, with the decrease in the relative cost of machinery to human labor and with the strict health regulations on some risky jobs, robots became credible alternatives to replace humans. For example, the refurbishment of the buildings that contain asbestos is still made by human workers, which subjects them to serious health hazards resulting from asbestos dust that can infiltrate into respiratory system even with the use of protections. Additionally, the productivity is an important issue and it cannot be limited to the human performance while the surface area of contaminated flats is considerable. Thus, the Robots to Re-Construction (Bots2ReC) project has started as an innovation action to efficiently automate the asbestos removal from real rehabilitation sites without endangering the human life ("Robots to Re-Construction", 2017). A mockup for grinding test is shown in Figure 1.

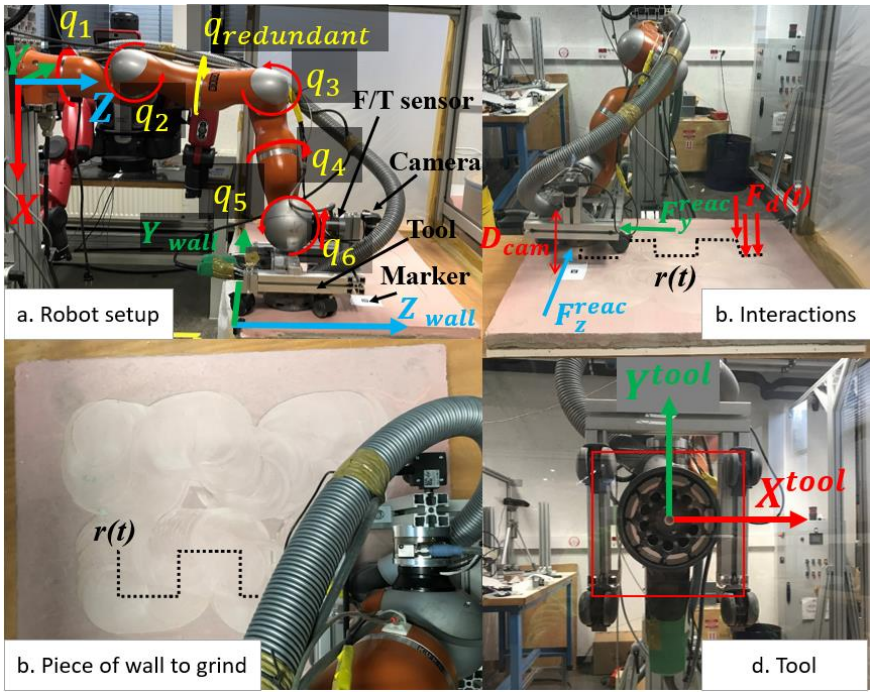

Figure 1: The robotic system equipped with a grinding tool, camera for distance measurement, and a force/torque sensor to perform grinding on a piece of wall

2 Control Framework

The control scheme presented in this paper uses three control subspaces (force-position-impedance) and can be applied to any robotic arm where position and orientation can be decoupled. In our modeling, the redundant joint of the Kuka LWR is blocked ($q_{redundant}$ in Figure 1a). Hence we are dealing with regular 6-dof, where hybrid position-force control that applies force along a desired trajectory can be achieved by the first three joints of the arm. The wrist joints are controlled by the Kuka impedance joint control to ensure the adaptation of the tool to the wall. The whole control block diagram is shown in Figure 2.

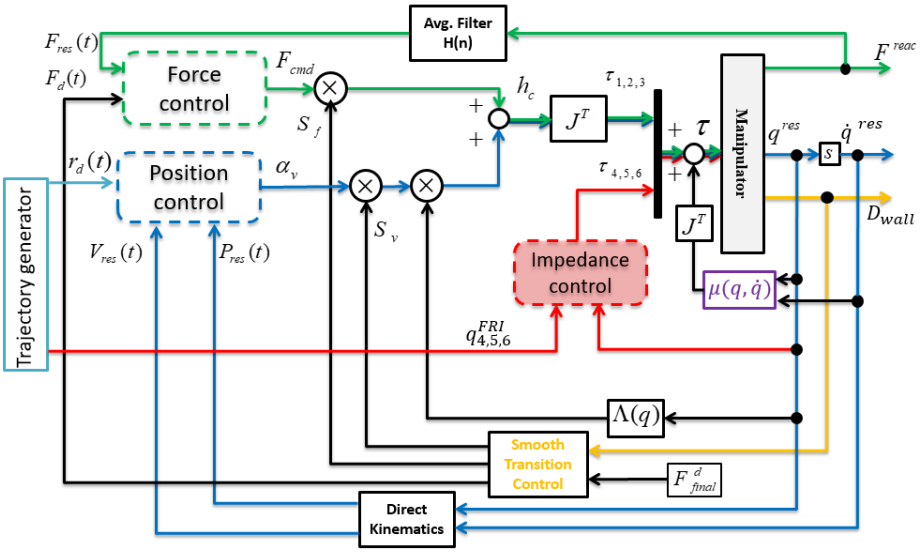

Figure 2: Hybrid controller block diagram: force control loop (green), position control loop (blue), impedance control loop (red) (refer to Section 2)

The control scheme is explained in the following subsections:

2.1 Hybrid Control in Operational Space

In order to accommodate unexpected interactions and irregularities of surfaces, the end-effector motion must be adapted by on-line modifications. Expressing a task in operational space requires a precise control of the end-effector motion, which can be achieved by the hybrid control proposed in (Siciliano, 2016). The controller can be expressed as follows:

$$h_c = \Lambda(q) S_v \alpha_v + S_f F_{cmd} + \mu(q, \dot{q}) \quad (1)$$

where $h_c \in R^n$ ($n = 3$ since the 1^{st} 3 joints were used) denotes the 3D forces of the center of the spherical joint in operational space; q corresponds to joint values, S_v and S_f are the diagonal selection matrices of position and force controlled directions

respectively; α_v and F_{cmd} are the acceleration and force commands respectively, $\Lambda(q)$ is the inertia matrix in task space defined by:

$$\Lambda(q) = (JH(q)^{-1}J^T)^{-1} \quad (2)$$

with J denoting the $(n \times n)$ kinematic Jacobian matrix, H is the $(n \times n)$ robot inertia matrix; μ is the $(n \times 1)$ function to compensate for Coriolis, gravitational and friction forces in the workspace. It is defined by:

$$\mu(q, \dot{q}) = \Gamma(q, \dot{q})\dot{q} + \eta(q) \quad (3)$$

where Γ is the wrench mapping the centrifugal, Coriolis and friction effects $c(q, \dot{q})$ from joint space into operational space:

$$\Gamma(q, \dot{q}) = J^{-T}c(q, \dot{q})J^{-1} - \Lambda(q)\dot{J}J^{-1} \quad (4)$$

and η is the wrench mapping the gravitational effects $g(q)$ from joint space into the operational space as:

$$\eta(q) = J^{-T}g(q) \quad (5)$$

Finally the joint torques τ can be calculated by:

$$\tau(q) = J^T h_c \quad (6)$$

The control loop expressed in (Equ.1) allows full decoupling between the force and velocity controlled subspaces (Figure 2).

2.2 Force and Position Control Loops

The desired force F_d can be achieved by setting:

$$F_{cmd} = F_d(t) + K_{PF}[F_d(t) - F_{res}(t)] \quad (7)$$

F_{cmd} is the command to force controller, F_{res} is the reaction force value and K_{PF} is positive-definite gain matrix. The proportional feedback is able to reduce the force error due to disturbance forces.
Position control can be achieved by imposing the acceleration α_v with:

$$\alpha_v = \ddot{r}_d(t) + K_{Dr}[\dot{r}_d(t) - V_{res}(t)] + K_{Pr}[r_d(t) - P_{res}(t)] \quad (8)$$

V_{res} and P_{res} are the velocity and position response of the end-effector from direct kinematics; K_{Dr} and K_{Pr} are suitable gain matrices; $\ddot{r}_d(t)$, $\dot{r}_d(t)$ and $r_d(t)$ are the desired operational acceleration, velocity and position tracking inputs, obtained from the trapezoidal trajectory generator with continuous acceleration as detailed in (Khalil, 2004).

2.3 Smooth Transition Control

The contact problem has been addressed in the literature (Volpe, 1991), (Zhou, 1998). In (Chang, 2002), the force was added after contact to reduce impact. In (Jamisola, 2002) motion control is used for approaching, then impact loading control was used to dissipate the impact force by setting the force command value negatively proportional to the velocity of the end-effector upon contact. In (Alkkiomaki, 2006), contact velocity is decreased based on vision and a rubber damper is added to reduce impact.
In our controller, to avoid the discontinuous switching between controllers and to reduce the impact force, a new strategy is introduced to change the selection matrix element $S(i,j)$ corresponding to the desired direction of motion from 0 to 1 smoothly ($i = j$, since S is diagonal matrix). This way, the controller inputs are continuous and the control flips smoothly from full position to hybrid control according to the distance from the grinding tool to the wall $D_{wall} = D_{cam} - d$. D_{cam} is the distance from the camera to the wall and d is the offset between the camera and the tool:

$$S_f(i,j) = e^{k_a * D_{wall}} \tag{9}$$

$$S_v(i,j) = 1 - S_f(i,j) \tag{10}$$

$$k_a = -\frac{log(S_{ffinal})}{D_{final}} + \varepsilon \tag{11}$$

$$\varepsilon = D_{final}^{wall} - D_{initial}^{wall} \tag{12}$$

S_{ffinal} is chosen as a small scalar close to 0, and the impact control is regulated by ε according to the distance range defined by $[D_{final}^{wall} - D_{initial}^{wall}]$. When $S_f(i,j)$ reaches 1, F_d goes from 0 to the maximum desired value as:

$$F_d(t) = \begin{cases} 0 & if \quad t \le t_{impact} \\ r_f(t - t_{impact}) + F_0 & if \quad t_{impact} < t \le t_{impact} + w \\ F_{final}^d & if \quad t > t_{impact} + w \end{cases} \tag{13}$$

where $r_f = \frac{F_{final}^d}{w}$ is the force rate, F_0 is the initial value of F^d and w is the desired period to reach the maximum force.

2.4 Impedance Control

The control law of the Kuka LWR joint specific impedance is:

$$\tau_j^{cmd} = k_i\left(q_j^{FRI} - q_j^{resp}\right) + D(d_i) + \tau_j^{FRI} \quad (14)$$

With this control law, a virtual spring $k_i\left(q_j^{FRI} - q_j^{resp}\right)$ can be realized in the joint level (Schreiber, 2010). τ_j^{cmd} is the low level torque sent to the motors, q_j^{FRI} is the desired joint value to be sent to the Fast Research Interface (FRI) that manages the communication between the Kuka LWR controller and the ordinary PC sending the desired commands, q_j^{resp} is the joint angular response. k_i and d_i are the stiffness and damping parameters for the joint j respectively. They can be modified from the remote side. τ_j^{FRI} is needed in case one needs to use torque based controllers to command the joints, for using the impedance controller τ_j^{FRI} is set to 0.

5 Experiments and Results

The control framework in Section 2 is implemented for a 7-R Kuka LWR robot using Robot Operating System (ROS) that communicates with the Kuka Fast Research Interface (FRI). The force sensor publishes data at a rate of 1000 Hz, the ROS control update loop and the trajectory node are updated at 500 Hz. The system was tested with a trapezoidal trajectory generator that provides continuous acceleration in the variable velocity phases and constant speed otherwise. The spindle runs with 11000 rpm, it rotates a disc with abrasive grains of 125 mm diameter. The robot is commanded to apply a force of 80 N on the desired path on the wall made of concrete and covered by a smoothing layer. The max velocity for the path was set to 0.015 m/s and the max acceleration was 0.1 m/s^2. The robot starts from free space and goes into the wall by a smooth transition from position to force control using the distance D_{wall} between the tool and the wall. D_{wall} is obtained using camera that detects a special pattern marker (Aruco marker) fixed on the wall with a precision of 1 mm, thus avoiding impact and maintaining the desired force. The impedance controller ensures centering the force on the tool and adapting its orientation to the wall. The controller gains used in the experiment are shown in Table 1.

Table 1 : Controller gains used in the test

Gain	K_{PF}	K_{Pr}	K_{Dr}	$k_i\ (N.m/rad)$	$d_i\ (N.m/rad)$
Value	1.2	1000	60	10	1

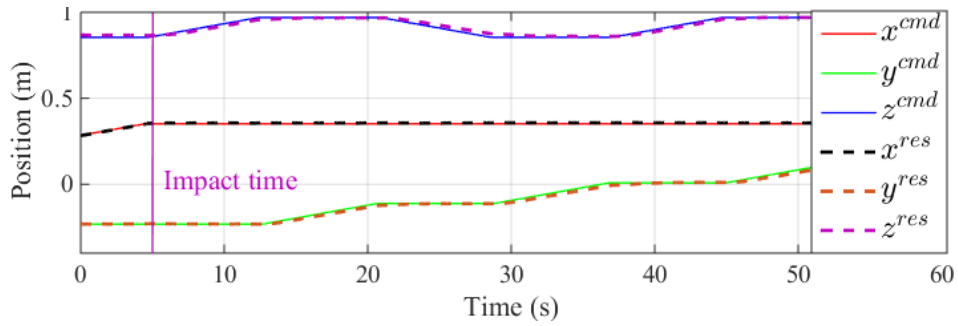

Figure 3 : Position command-response

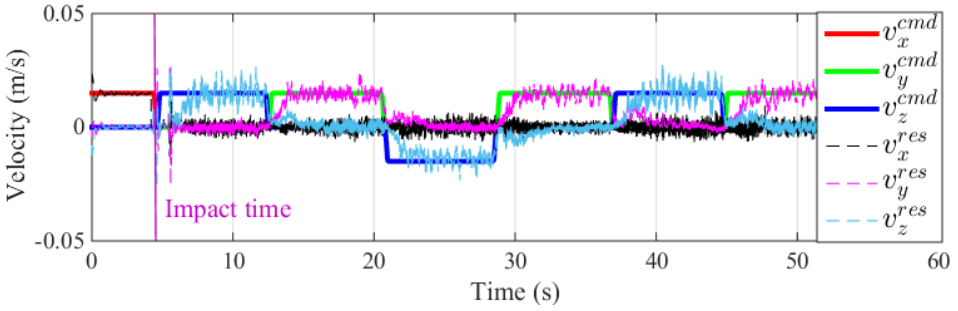

Figure 4: Velocity command-response

The command and response of tool trajectory position and velocity are shown in Figure 3 and Figure 4 respectively. The controller shows good performance in free space and after contact, the position error along the *X* direction is 2 mm at maximum, and relatively small compared to *Y* and *Z* directions where the errors reaches 19 mm and 9 mm respectively as shown in Figure 5, this is due to the insufficient force capacity of the arm. This variation in position errors is due to the lateral forces on the tool (Figure 1b & Figure 6). For the force control, since the sensor data needed for the feedback is very noisy because of the vibrations (Figure 6), a moving average filter $H(n) = \sum_1^n F^{reac}(n)/n$ with n=200 samples is used for smoothing. The force command versus response are plotted in Figure 7. The control with smooth transition shows negligible impact force when touching the wall, thanks to the transition control presented in 2.3 that flips smoothly from position into force control in a unified manner that avoids switching as Figure 9 shows. The desired force reference value is reached in a behavior similar to a step function. The force value is maintained along the path with an error less than 10 N as shown in Figure 8.

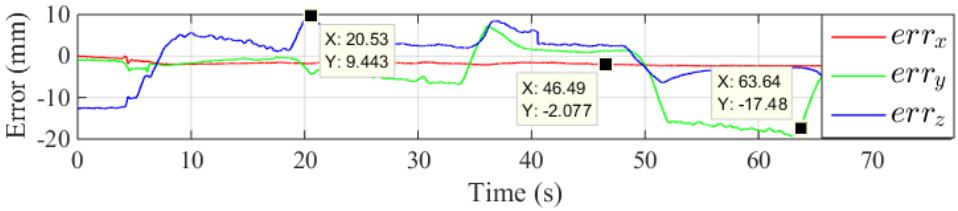

Figure 5 : Position command-response errors

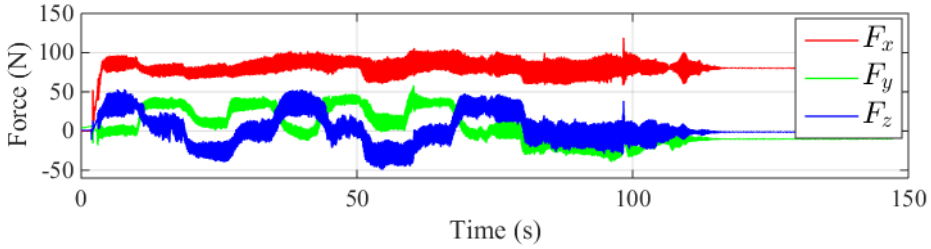

Figure 6: Reaction forces on the tool while grinding

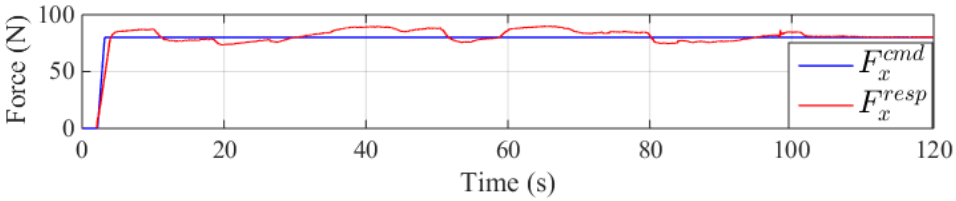

Figure 7: The command and response of normal force on the wall

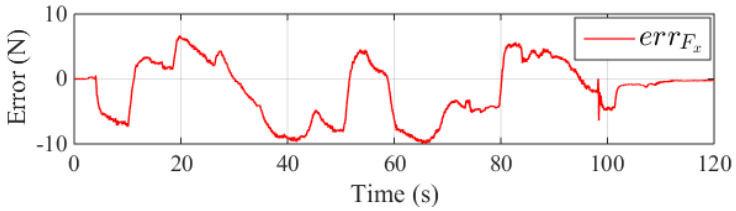

Figure 8: Normal force command-response errors

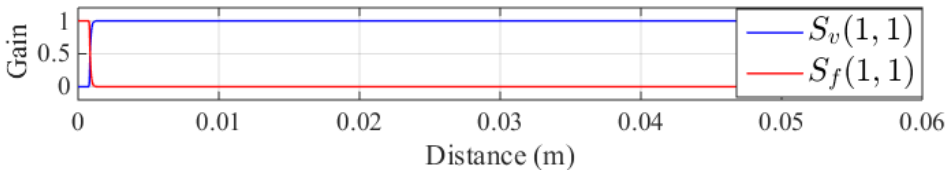

Figure 9: Smooth switching from position to force control. (1,1) is the index to the first element of the selection matrix

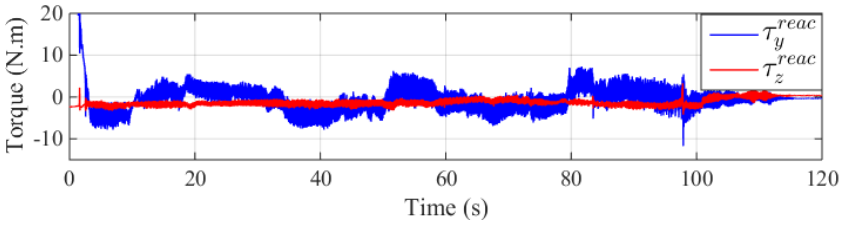

Figure 10: The reaction torques on 5th and 6th joints

As described 2.4, the wrist motors are controlled by impedance (Equ.14). The controller gains shown in Table 1 are used to ensure stability and equivalent distribution of contact forces. The effectiveness of the impedance controller in adapting the tool to the wall, can be deduced from the fact of keeping minimal torques on 5th and 6th joints that are

responsible for the pitch and yaw of the tool as Figure 10 shows. Figure 11 shows how the controller maintains the force inside the tool frame as the zero-moment-point of the tool-wall contact is inside the frame of the tool. The only exception corresponds to the first contact, where the controller tries to overcome the relatively high lateral forces.

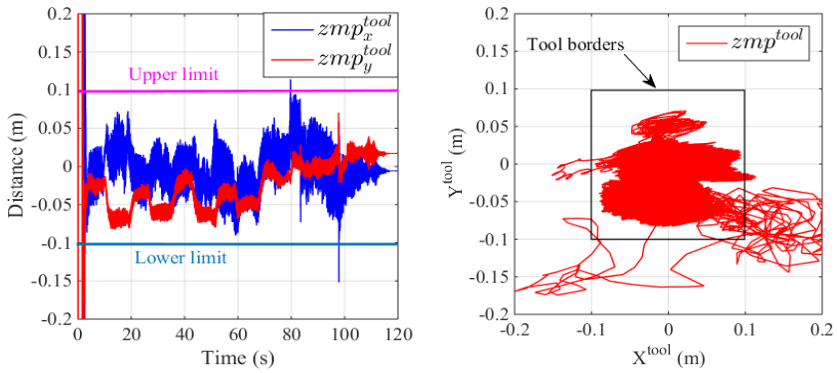

(a) Zmp coordinates **(b) Zmp trajectory**

Figure 11: Zero-moment-point on the end-effector expressed in the tool frame shown in Figure 1d

6 Conclusion

This article presents experimental validation of a smooth position-force hybrid controller that can reactively adapt to the environment while grinding. The controller is tested on Kuka LWR using camera and force-torque sensor for tracking the surfaces while trying to maintain a desired force centered on the disc and normal to the surface. The smooth transition control showed that the switching problem can be overcome. The controller changes smoothly between free space and contact modes, thus reducing impact force close to zero and avoiding uncertainties. The results of position and force tracking performances are acceptable and impact force is close to zero. In near future, the controller will be updated using active orientation control to better overcome the lateral forces and keep the normal force centered on the tool. Future tests will be also transposed on a stiffer and stronger arm designed by the Bots2ReC consortium. Some identification tests are planned as well to determine the best combination between the linear velocity of grinding, the depth of the cut and the force needed for grinding.

Acknowledgements

"The research leading to these results has received funding from the European Union's Horizon 2020 research and innovation programmes under grant agreement No. 687593"

References

Alkkiomaki, O., Kyrki, V., Kalviainen, H., Liu, Y., & Handroos, H. (2006, December). Smooth transition from motion to force control in robotic manipulation using vision. In Control, Automation, Robotics and Vision, 2006. ICARCV'06. 9th International Conference on (pp. 1-6). IEEE.

Chang, W. C., & Wu, C. C. (2002). Integrated vision and force control of a 3-DOF planar robot. In Control Applications, 2002. Proceedings of the 2002 International Conference on (Vol. 2, pp. 748-753). IEEE.

IFR (2016). Executive summary world robotics 2016 service robots. Retrieved June 07, 2017, from https://ifr.org/downloads/press/02_2016/Executive_Summary_Service_Robots_2016.pdf, 2016/

Jamisola, R., Ang, M. H., Oetomo, D., Khatib, O., Lim, T. M., & Lim, S. Y. (2002). The operational space formulation implementation to aircraft canopy polishing using a mobile manipulator. In Robotics and Automation, 2002. Proceedings. ICRA'02. IEEE International Conference on (Vol. 1, pp. 400-405). IEEE.

Khalil, W., & Dombre, E. (2004). Modeling, identification and control of robots. Butterworth-Heinemann.

Mohy El Dine, K., Corrales, J. A., Mezouar, Y., & Fauroux, J. C. (2017, December). A Smooth Position-Force Controller for Asbestos Removal Manipulator. IEEE International Conference on Robotics and Biomimetics (ROBIO), Macau, 2017 (to appear).

Robots to Re-Construction (Bots2ReC). (n.d.). Retrieved December 11, 2017, from http://www.bots2rec.eu/

Schreiber, G., Stemmer, A., & Bischoff, R. (2010, May). The fast research interface for the kuka lightweight robot. In IEEE Workshop on Innovative Robot Control Architectures for Demanding (Research) Applications How to Modify and Enhance Commercial Controllers (ICRA 2010) (pp. 15-21). Citeseer.

Siciliano, B., & Khatib, O. (Eds.). (2016). Springer handbook of robotics. Chapter 7 (pp.161-185) Springer.

Volpe, R., & Khosla, P. (1991, April). Experimental verification of a strategy for impact control. In Robotics and Automation, 1991. Proceedings., 1991 IEEE International Conference on (pp. 1854-1860). IEEE.

Zhou, Y., Nelson, B. J., & Vikramaditya, B. (1998, May). Fusing force and vision feedback for micromanipulation. In Robotics and Automation, 1998. Proceedings. 1998 IEEE International Conference on (Vol. 2, pp. 1220-1225). IEEE.